metals

MDPI

Article

Crystal Chemistry at Interfaces Between Liquid Al and Polar SiC{0001} Substrates

Changming Fang * and Zhongyun Fan

Brunel Centre for Advanced Solidification Technology (BCAST), Brunel University London, Uxbridge UB8 3PH, UK; zhongyun.fan@brunel.ac.uk

* Correspondence: changming.fang@brunel.ac.uk

Abstract: Silicon carbide (SiC) has been widely added into light metals, e.g., Al, to enhance their mechanical performance and corrosion resistance. SiC particle-reinforced metal matrix composites (SiC-MMCs) exhibit low weight/volume ratios, high strength/hardness, high corrosion resistance, and thermal stability. They have potential applications in aerospace, automobiles, and other specialized equipment. The macro-mechanical properties of Al/SiC composites depend on the local structures and chemical interactions at the Al/SiC interfaces at the atomic level. Moreover, the added SiC particles may act as potential nucleation sites during solidification. We investigate local atomic ordering and chemical interactions at the interfaces between liquid Al (Al(l) in short) and polar SiC substrates using ab initio molecular dynamics (AIMD) methods. The simulations reveal a rich variety of interfacial interactions. Charge transfer occurs from Al(l) to C-terminating atoms (Δq = 0.3e/Al on average), while chemical bonding between interfacial Si and Al(l) atoms is more covalent with a minor charge transfer of Δq = 0.04e/Al. The prenucleation at both interfaces is moderate with three to four recognizable layers. The information obtained here helps increase understanding of the interfacial interactions at Al/SiC at the atomic level and the related macro-mechanical properties, which is helpful in designing novel SiC-MMC materials with desirable properties and optimizing related manufacturing and machining processes.

Keywords: ceramic–metal interfaces; liquid-Al/SiC interfaces; prenucleation; interfacial interactions; ab initio molecular dynamics

check for updates

Citation: Fang, C.; Fan, Z. Crystal Chemistry at Interfaces Between Liquid Al and Polar SiC{0001} Substrates. *Metals* **2024**, *14*, 1258. https://doi.org/10.3390/met14111258

Academic Editors: Wislei Riuper Osório and Mauro Giovannini

Received: 26 September 2024
Revised: 26 October 2024
Accepted: 4 November 2024
Published: 6 November 2024

Copyright: © 2024 by the authors. Licensee MDPI, Basel, Switzerland. This article is an open access article distributed under the terms and conditions of the Creative Commons Attribution (CC BY) license (https://creativecommons.org/licenses/by/4.0/).

1. Introduction

Silicon carbide (SiC) is a ceramic material. It exhibits advantageous properties, such as high hardness, good fatigue resistance, high thermal conductivity, low coefficient of thermal expansion, high chemical inertia, and resistance to corrosion [1,2]. Thus, SiC has many applications, including in automotive water pump seals, bearings, pump components, and extrusion dies [1–4]. Moreover, SiC has a mass density of 3.2 g/cm^3 [2–4], which is comparable with that of Al (2.7 g/cm^3) [5]. It has thus been utilized as an additive into light metals, such as Mg and Al, to manufacture (nano-sized) SiC particle-reinforced metal matrix composites (SiC-MMCs). SiC-MMCs display excellent mechanical performance, high corrosion resistance, and high volume/weight ratios [6–9]. They have potential applications in aerospace, automotives, etc. [8–10].

Experimental efforts have been focused on the preparation of SiC particle-enhanced composites, e.g., Al metal matrix composites (Al/SiC-MMCs) with different SiC contents [8–11], developments of preparation techniques, and properties measurements [6–10]. Recently, experimentalists worked hard at machining Al/SiC-MMCs and found various phenomena related to Al/SiC interfaces, such as matrix deformation and debonding between Al and SiC substrates [9–11]. These macroscopic properties of Al/SiC-MMCs originate from local atomic arrangements and interfacial chemical bonding. Knowledge about local crystal chemistry at the interfaces between liquid Al metal and SiC substrate surfaces is therefore

vital to understand their macro-mechanical properties and applications and to understand the related manufacturing and machining processes.

Along the [0001] orientation, the structures of the hexagonal (4H-, or 6H-) SiC forms consist of SiC double-atom layers which can be regarded as the building blocks [1,12]. Rich SiC polytypes originate from the different stackings of SiC blocks. Each atom is tetrahedrally coordinated by the other species: three in the double-atom layer and one in the neighboring layer. Both Si and C atoms in the structures satisfy the sp^3 bonding. The unusual SiC structure indicates that cleaving the structure between the SiC double-atom layers is easier for creating SiC{0001} substrate surfaces. In this way, the produced SiC{0001} substrate surface is terminated either by C or by Si. In chemistry, the electronegativity is 1.90 in Pauling scale for silicon and 2.55 for carbon, respectively. Such a large electronegativity difference results in the created SiC{0001} surfaces having a polar nature, making them unstable at ambient conditions [13]. Fortunately, it is different in (liquid) metals since the free electrons of the metal atoms balance the polarity of the substrate surfaces [14,15]. Meanwhile, it is expected that the orientational sp^3 bonding of the outmost Si and/or C atoms with one dangling bond has impacts on the atomic ordering in the liquid adjacent to the substrates and the interfacial chemical bonding.

Above its nucleation temperature, there is atomic ordering in the liquid adjacent to a solid substrate [14,15]. This phenomenon is referred to as prenucleation [16,17]. Prenucleation supplies a precursor for following nucleation, which is crucial for solidification [18]. Such atomic ordering relates to interfacial bonding. The atomic arrangements of liquid Al atoms adjacent to the substrates and interfacial chemical bonding remain during casting [14,16,17]. Interfacial chemical bonding largely determines the mechanical properties of SiC-MMCs. Information about the local structure and chemical interaction at the liquid/solid interfaces thus helps us understand not only the nucleation potency of, e.g., the SiC substrates, but also the mechanical and chemical performances of the cast products [9,19] and the Al matrix deformation and interface debonding between the Al and SiC while machining SiC-MMCs.

Experiments have been conducted to understand the local structure at Al/SiC interfaces using various techniques, including high-resolution electron microscopy (HR-TEM) [20–22]. The HR-TEM images provided significant information about the atomic arrangements at the interfaces for the prepared samples. However, the obtained knowledge is mainly on the averaged atomic arrangements and is far from complete. In this aspect, theoretical approaches, especially parameter-free first-principle/ab initio methods, have advantages. This has been evidenced by previous studies on the assorted interfaces between liquid metal and solid substrates [14,15,23,24]. There have been reports on first-principles calculations for the interfaces between solid Al and SiC{0001} substrates with 3C- [25], 4H- [26,27], or 6H-stackings [28–31]. The calculations revealed stronger chemical interactions between the Al- and C-terminated substrates than between Al- and Si-terminated interfaces. Wang and Chen [32] performed atomistic modeling on misfit dislocations at the interfaces between SiC and several metals, including Al, using the potentials derived from ab initio calculations. Recently, ab initio molecular dynamics (AIMD) simulations were performed for the interfaces between liquid Mg and SiC{0001} substrates, and atomic ordering was observed in the liquid Mg near the SiC substrates [33]. Moreover, the simulations found atomic vacancies at the Mg layer adjacent to the substrates. To date, there is no report on the local structure and chemical interactions at the interfaces between liquid Al and SiC substrates (in short, Al(*l*)/SiC interfaces). Here, we investigate the atomic ordering/prenucleation and interfacial chemical bonding at the Al(*l*)/SiC{0001} interfaces using AIMD methods. Electronic band structure calculations are performed for equilibrated configurations. Bader charge analysis is employed to obtain the interface charge transfer between the liquid Al atoms and the substrate atoms based on the electron density distribution at the interfaces from the band structure calculations. This study reveals a rich variety of atomic ordering in the liquid Al atoms adjacent to the substrates and interfacial chemical interactions. There is a notable charge transfer from Al(*l*) to C-terminating atoms. Meanwhile, interfacial Si

and Al(*l*) atoms exhibit more covalent interactions. The information obtained here helps us understand the interfacial interactions of Al/SiC at the atomic level, which relates to the macro-mechanical properties of SiC-MMC materials and helps us design novel MMCs and related manufacturing and machining processes.

2. Methods

The ab initio approach employed in this study utilizes the periodic boundary conditions [34]. Thus, the usage of supercells is required. A hexagonal supercell was created with $a = 5a_0$, where a_0 is the length of the a-axis of the conventional hexagonal cell of 4H-SiC with consideration of the thermal expansion at the simulation temperature [33,35]. The c-axis is determined by the thickness of the SiC slab and the volume of the Al atoms with the density at the simulation temperature [5]. A supercell with a = 15.53 Å and c = 43.83 Å for the Al(*l*)/SiC{0001} interfaces was obtained accordingly. This cell contains 400 Al(*l*), and the substrate contains 100 Si and 100 C. The input interface model is shown schematically in Figure 1a. Such a sizable supercell helps attain statistically meaningful results and avoid the risks of artificial crystallization in the liquid metal.

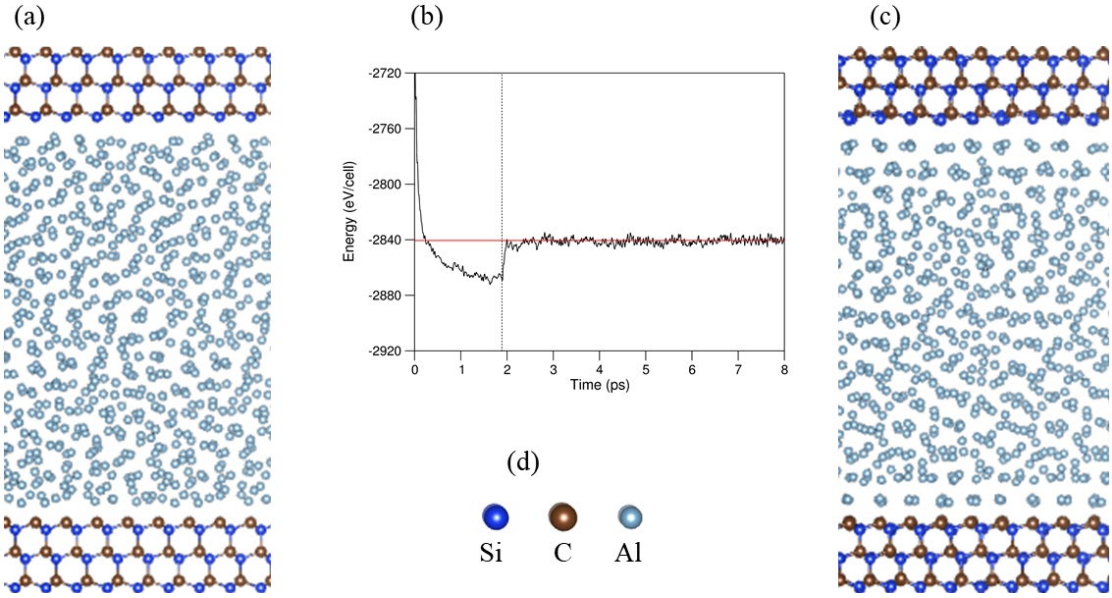

Figure 1. A schematic of the input structure (**a**), the relation between the total valence electron energy and simulation duration (**b**), and a snapshot of L-Al/SiC{0001} interfaces equilibrated at 1000 K (**c**). The meaning of the spheres (**d**) for (**a**,**c**) is as follows: the blue spheres represent Si, dark brown represents C, and silver represents Al. The liquid Al atoms adjacent to the substrates exhibit atomic ordering, and they are solid-like.

A plane-wave pseudo-potential path within the first-principle's code VASP was utilized [34,36]. This code employs the electronic density functional theory within the projector-augmented wave framework [37]. The generalized gradient approximation created by Perdew, Burke, and Ernzerhof (GGA-PBE) [38] was used for the exchange and correlation terms. The cut-off energies are E_{CUT}/E_{AUG} = 520.0 eV/700.0 eV. These values are higher than the default values of the atoms (E_{MAX}/E_{AUG} = 240.3 eV/291.1 eV for Al, 245.3 eV/322.1 eV for Si, and 400.0 eV/644.9 eV for C, respectively) for electronic structure calculations.

For the AIMD simulations, a cut-off energy of 320.0 eV was employed. This energy value is reasonable compared with the E_{MIN} values of the pseudopotentials of the related atoms. The Γ-point in the Brillouin zone was used [39]. The latter is due to the lack of periodicity of the whole Al(*l*)/SiC system. The AIMD simulations were carried out utilizing the NVT ensemble [34,36].

Liquid Al samples were produced first by equilibrating for about 3 ps (picoseconds) at 3000 K. Then, they were quenched to the designed temperature. The obtained liquid Al samples were inserted into the space between the SiC{0001} surfaces. A vacuum of about 2.0 Å was created between the surface of the liquid and the substrates (Figure 1a). AIMD simulations were performed via a two-step method. First, AIMD simulations were carried out with the substrate atoms pinned for over 1000 steps (1.5 fs (femtoseconds) per step). Then, the simulations were continued with full relaxation of the atoms for another 4000 steps. Analysis found no notable changes in atomic ordering at the interfaces. This two-step path prevents possible collective atomic movements which may occur when all atoms are relaxed from the start. The samples of the interfaces over 3.0 ps were used to ensure the results were statistically meaningful [34,40].

3. Results

Figure 1a shows the schematic structure of the input Al(*l*)/SiC interfaces, the model of which is described in the above section. There is a space between the solid substrates and the liquid Al at each side. The Al atoms display no long-range ordering. The ab initio calculations reveal a high total valence electron energy at $t = 0$ (Figure 1b).

When the simulation starts, the liquid Al atoms move around. The Al atoms at the borders move towards the fixed substrate atoms, gradually forming chemical bonding with the atoms at the substrate surfaces. Consequently, the energy decreases quickly in the first 0.3 ps and then decreases more smoothly until it reaches a constant value at about 1.6 ps (Figure 1b). Releasing the substrate atoms raises the energy dramatically. The energy reaches the equilibrium value within another 0.5 ps. Then, the energy varies around the equilibrium value. We equilibrated the system for another 5 ps. During the AIMD simulations, the substrate atoms vibrate around their equilibrium positions, remaining solid-like. An analysis revealed that from about 3.0 ps, the overall structure of the Al atoms remains unchanged. A snapshot of the equilibrated Al(*l*)/SiC{0001} system at 1000 K is presented schematically in Figure 1c.

Figure 1c shows obviously that the substrates' atoms and the (liquid) Al atoms are well-separated. The substrate atoms are well ordered and behave like they are in a solid phase at the simulation temperature. Meanwhile, the Al away from the interfaces displays no long-range ordering, and it is liquid-like. The Al atoms adjacent to the substrates exhibit localization, which decreases with the distance from the substrate surfaces. A closer look at Figure 1c shows the atomic density changing with an increasing distance from the surfaces. This phenomenon that atomic density varies with distance from the substrate in the direction perpendicular to the substrates is defined as layering. Layering can be described using the atomic density profile (ADF) [16,17,33,41]. An analysis for the equilibrated configurations over 3 ps was carried out, and the results are shown in Figure 2a. Variations in the peak heights for the layers around the interfaces are shown in Figure 2b.

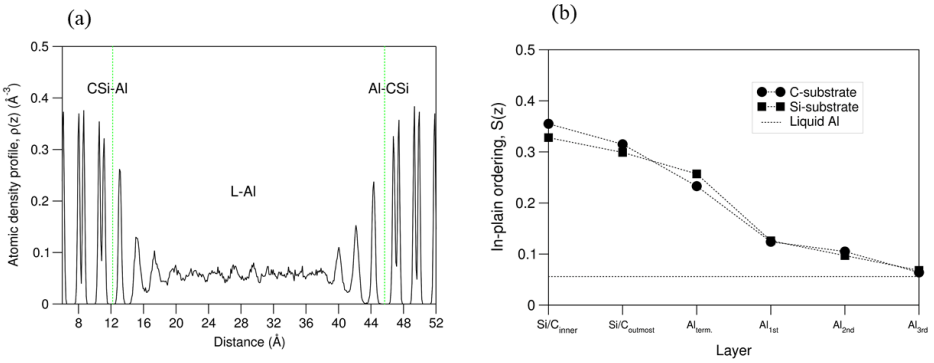

Figure 2. The atomic density profile, ρ(z) (**a**), and the variation in the peak heights of atomic layers (**b**). The straight dotted straight in (**b**) shows the average Al(*l*) density. The Al atoms adjacent to the SiC substrates form sharp layers.

Figure 2a shows sharp peaks for the Si and C atoms in the substrates, corresponding to their solid-like nature (Figure 1c). The termination Al atoms at both interfaces form peaks at 13.1 Å and 44.3 Å, respectively. These peaks are well separated from the neighboring layers. The ADF peak heights of the Al layers decrease with an increasing distance from the interfaces. The density of the third Al layer at both interfaces is just above the average Al(l) value (Figure 2b). There are three recognizable Al peaks near the Si substrate. Near the C substrate, there are three to four apparent Al(l) peaks, but the fourth peak is rather weak (Figure 2a). This indicates that layering phenomenon at the Al(l)/SiC{0001} interfaces (three to four layers) is moderate. The analysis also showed that the peak distance between the outmost C-layer and the Al$(l)_{\text{term}}$ layer is 1.8 Å, which is shorter than that between the outmost Si-layer and the terminating Al layer (2.0 Å).

In the heterogeneous nucleation of light metals, solid grows layer by layer [42]. The atomic ordering in the liquid metals adjacent to the substrates acts as a template for the nearby liquid to nucleate. The atomic arrangements in the layers near the substrates for the equilibrated configurations over 3 ps are analyzed and shown in Figure 3.

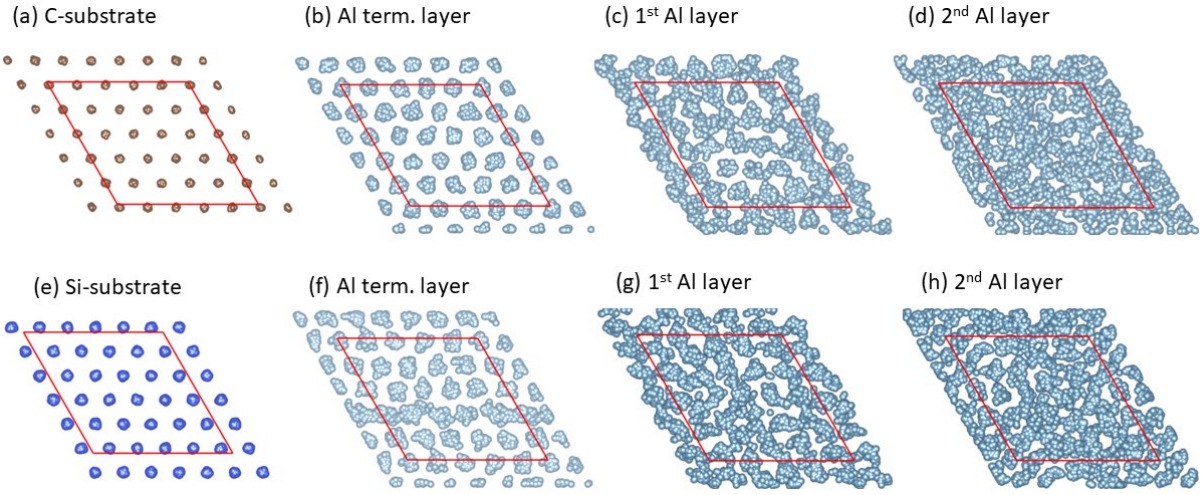

Figure 3. Averaged atomic arrangements of the outmost substrate layer and the Al layers at the C-terminated (**a**–**d**) and the Si-terminated (**e**–**h**) substrates over 3 ps. The red lines represent the in-plane axis for the supercells. The blue spheres represent Si, dark brown represents C, and silver represents Al. The terminating Al atoms (**b**,**f**) are highly ordered. The ordering of the terminating Al atoms at the C-terminating interface (**b**) is more significant than that at the Si-terminated interface (**f**).

To assess the ordering of the atoms in the layers near the substrates, an in-plane ordering coefficient [14,15,33,41] was employed for the configurations over 3 ps. The results are plotted in Figure 4.

From Figures 3 and 4, we obtained the following results:

(i) Both the surface C (Figure 3a) and Si (Figure 3e) atoms in the substrates are well ordered and solid-like. Their in-plane ordering coefficients are close to each other and to those in the substrates (Figure 4).

(ii) The terminating Al atoms at both substrates are highly ordered (Figure 3b,f), which corresponds well to the sharp ADP peaks and sufficient separation from the neighboring atoms (Figure 1b,c and Figure 2a). There are some subtle differences in atomic arrangements in the two terminating Al layers. The terminating Al atoms on the C substrate are separated from each other and show a localized nature, while some of the terminating Al atoms above the Si-terminated substrate show higher mobility and are connected to each other in the averaged arrangements (Figure 3f). Correspondingly, the in-plane ordering coefficient of the terminating Al atoms at the Si-terminated substrate is about 0.22, which is lower than that at the C-terminated substrate (0.31). The first Al layers at both substrates (Figure 3c,g) exhibit moderate atomic ordering, with the in-plane ordering coefficients being about 0.03.

There is little atomic ordering for the Al atoms at the second layer at both substrate surfaces, as shown in Figure 3d,h and Figure 4.

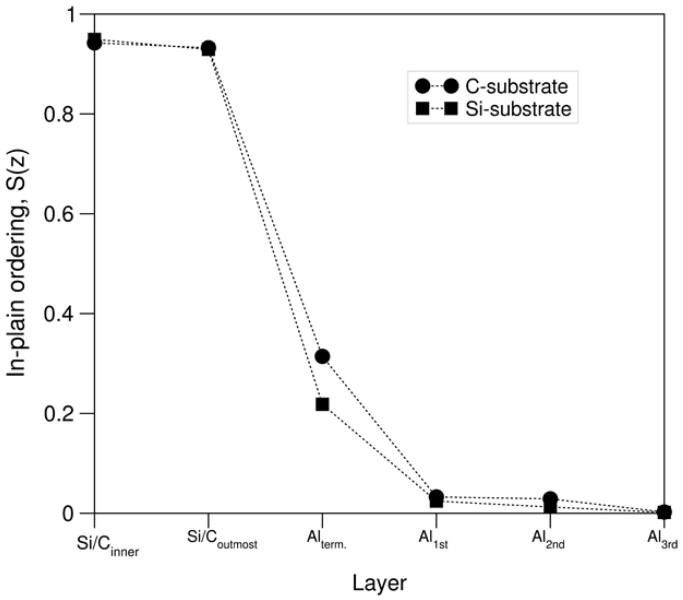

Figure 4. The in-plane ordering coefficients for the atomic layers nearby the L-Al/SiC{0001} interfaces. The *S*(z) value for the terminating Al atoms at the C-terminated interface is higher than that at the Si-terminated interface.

We make statistics of atoms at each layer. The atomic ratio between those at the Al layer (n(Al)) and the substrate layer (n(C)), n(Al)/n(C), is 1.00 for the terminating Al layer, 1.05 for the first Al layer, and 1.13 for the second Al layer for the C-substrate. At the Si-terminated substrate, the corresponding ratios of n(Al)/n(Si) are 1.03, 1.06, and 1.13 for the terminating Al and the first and second Al layers, respectively. The atomic density of the second Al layer is close to the bulk values of the liquid Al misfit between a[SiC{0001}]/a[Al{111}] ~ 1.06 at the melting temperature of liquid Al, which corresponds to an area ratio of 1.13 [5].

The above results indicate stronger interfacial chemical bonding between C-Al than between Si-Al. The value of the atomic ratios at the interfaces is about 1, indicating that the majority of the outmost C/Si atoms have one Al neighbor, forming distorted tetrahedral coordination. Here, we analyzed the interfacial chemical interactions and chemical bonding in more detail. The atomic arrangements and local bonds at the C-substrate (Figure 5a) and the Si-substrate (Figure 5b) and the typical local coordination of the surface C (Figure 5c) and Si (Figure 5d) atoms are schematically presented, respectively.

Figure 5 shows that the terminating C or Si atoms have one Al atom as the nearest neighbor, forming a distorted tetragonal coordination which satisfies the sp^3 hybridization together with the three Si/C neighbors in the subsurface layer, according to Pauling's theory [43].

To obtain a deeper understanding of the local chemical interactions at the interfaces, we performed electronic band structure calculations for the Al(l)/SiC system. The obtained electron density distributions are shown in Figure 6a. Based on the electron density distributions, we also analyzed the charges at the atomic sites at the interfaces using Bader's charge analysis model [44]. The obtained charges at the atomic sites at the interfaces are shown in Figure 6b. Moreover, we plotted the partial density of states for selected atoms at the interfaces in Figure 7.

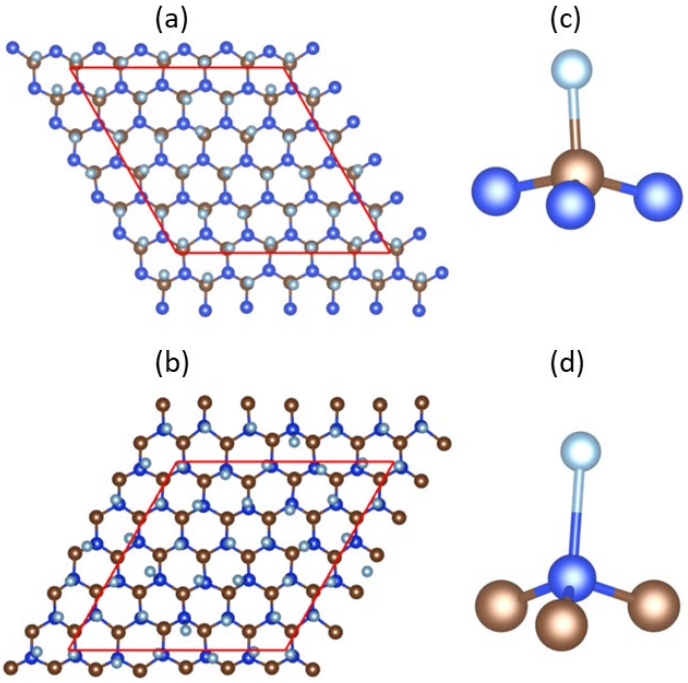

Figure 5. The atomic ordering of the terminating Al layer and the SiC surface layers with the C-termination substrate (**a**) and the Si-termination substrate (**b**) and the typical local coordination of the surface C (**c**) and Si (**d**) atoms. The red lines in (**a**,**b**) represent the in-plane axis. The blue spheres represent Si, dark brown represents C, and silver represents Al.

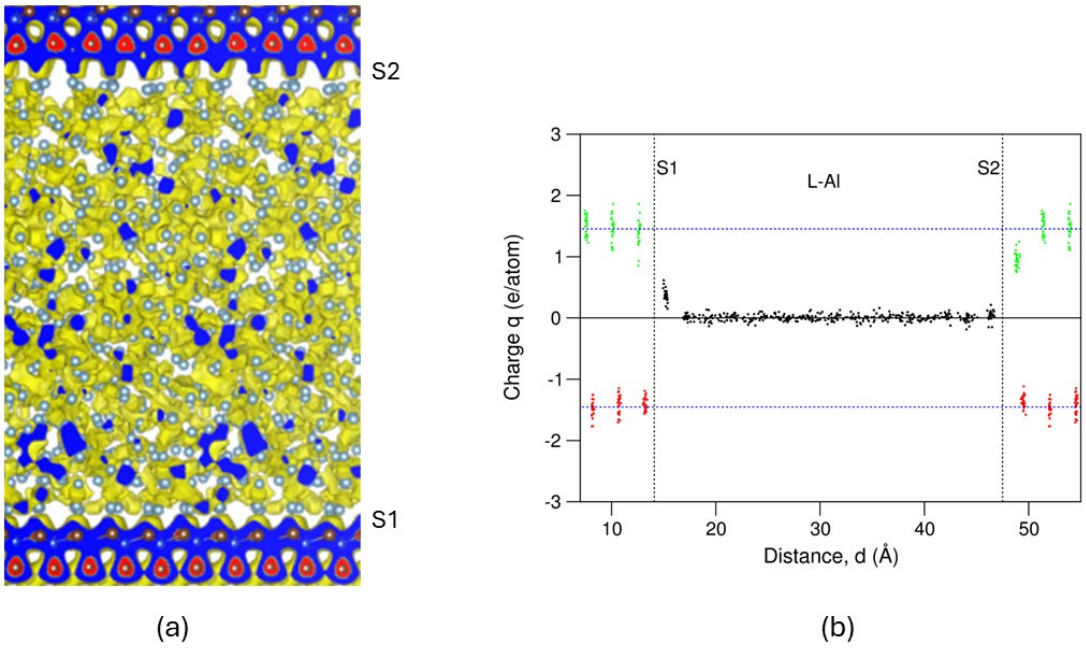

Figure 6. Electron density iso-surfaces with $\rho_0(r) = 0.035e/Å^3$ (**a**) and related Bader charges at the atomic sites (**b**). In 6a, the yellow clouds represent the iso-surfaces. The blue color represents regions with higher electron densities, and white represents regions with lower electron densities. The red regions represent the core regions of intensive electron densities. The blue spheres represent Si, dark brown represents C, and silver represents Al. In (**b**), the red dots represent charges at C, the green represents charges at Si, and black represents charges at Al. The charge transfer at the C-terminated interface (S1) is notably higher that at the Si-terminated interface (S2). All the snapshots and electron density iso-surfaces were produced via the program VASTA [45].

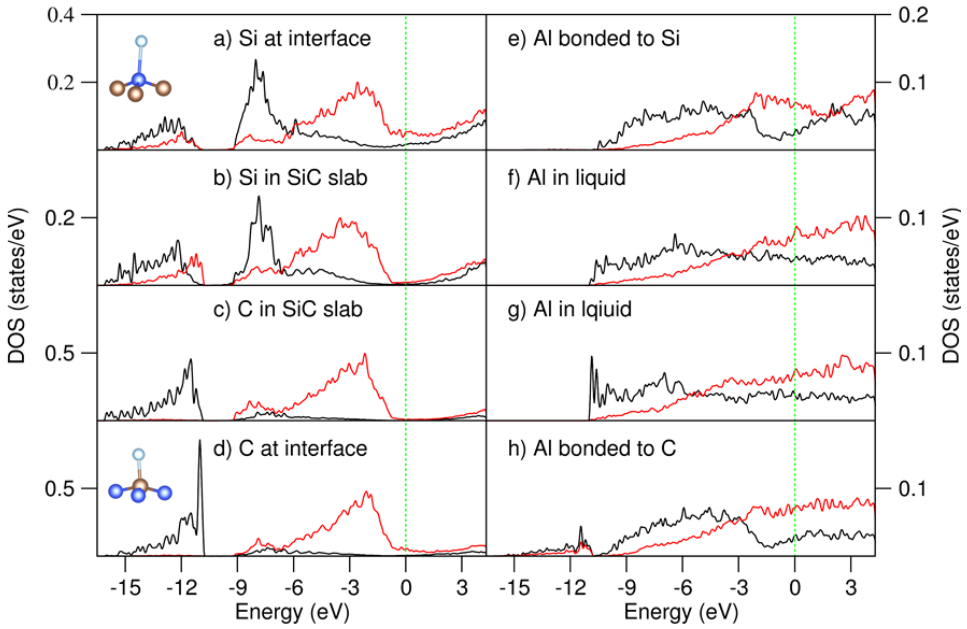

Figure 7. The partial density of state (pDOS) curves of selected atoms in the L-Al/SiC{0001} interfaces. The black curves represent the s-characters, and red represents the p-characters.

Figure 6a shows the localized electrons around the Si/C atoms in the substrates, while the Al atoms show its naked ions with (free) electrons around them. This corresponds to the strong Si-C covalent bonding and the free-electron nature of Al metals. Figure 6b shows the results of interatomic charge transfer from the Bader analysis. The Si atoms in the substrate are positively charged with a loss of about 1.5e/Si, whereas the C atoms obtained the same amount of electrons. The Al atoms away from the substrates are electronically neutral.

Figure 6b shows the occurrence of interfacial charge transfer (0.3e/Al on average) from the terminating Al atoms to the C-terminated substrate. Meanwhile, the terminating Al atoms lost little electrons (<0.1e/Al on average) to the outmost Si atoms. It is also noted that the outmost Si atoms lost fewer electrons than those in the substrate bulk. Those results are in good agreement with the electronegativity values, which are 2.5 for C, 1.8 for Si, and 1.5 for Al in Pauling's scale. The moderate charge transfer between Al and Si atoms corresponds to their more covalent interactions (the difference in electronegativity values is 0.3) compared with that between C and Al (the difference is 1.0).

Figure 7 shows the curves of the partial density of states for selected atoms around the interfaces. Around the Fermi level (zero eV), the electron densities of the Si (Figure 7b) and C (Figure 7c) in the center of the substrate slab are very low and more like pseudo-gaps. This corresponds to the semiconducting nature of SiC [4]. Meanwhile, there are nonignorable densities of states around the Fermi level for the outmost Si (Figure 7a) and C (Figure 7d). An analysis revealed that they originate from interfacial chemical interactions. Figure 7d shows a sharp peak at the top of the C 2 s states at −11.0 eV, which arises due to the C-Al interaction, as shown in Figure 7h, where there are some Al 3 s 3p states at the same energy range. Figure 7f,g show free-electron-like DOS curves for the Al atoms in the center of the Al slab. Even the partial density of states curves for the Al near the outmost Si (Figure 7a) shows weak densities in the low Si 3 s, 3p part between −15.5 eV and −11.0 eV. This indicates weak chemical bonding between the Al and Si atoms. The notable densities of states of the Si atom (Figure 7a) are the tails of the neighboring Al atoms.

4. Discussion

The AIMD simulations and electronic band structure calculations provided information about the local structures and interfacial interactions at the Al(*l*)/SiC{0001} interfaces. Each of the terminating C atoms is bonded to one Al, and thus, every C atom terminating

the substrate has four (three Si and one Al) neighbors, fulfilling sp^3 hybridization. The interfacial interactions between Al and the terminating C atoms are strong with a charge transfer of about 0.3e/Al from Al to C (as summarized in d in Table 1). Therefore, energy costs for debonding at the Al(l)/SiC{0001}$_C$ interfaces will be high.

This study also showed anisotropy of chemical bonding at the interfaces: the bond between Al and the Si atoms terminating the substrate is relatively weaker and covalent compared to that between C and Al. There is a minor charge transfer from the terminating Al atoms to the Si atoms terminating the substrate (0.04e/Al on average; see e in Table 1). Moreover, the simulations also showed mobility of the terminating Al atoms, and there are some extra Al atoms in the terminating Al layer, with the n(Al)/n(Si) ratio being about 1.03. Such weaker Si-Al bonding means easier interfacial debonding at the Al/SiC{0001}$_{Si}$ interfaces during machining.

Prenucleation at a liquid metal/solid substrate interface is associated with the intrinsic capability (potency) of the substrate [46,47]. There are four factors affecting prenucleation at a solid metal/liquid substrate interface at a temperature above the nucleation point, including (i) the temperature, T [17]; (ii) the lattice misfit between the substrate and the metal, f [16,47]; (iii) the interfacial chemical interaction [17]; and (iv) the atomic roughness of the substrate, R [24,46–48]. The interfacial interaction can be scaled by charge transfer at the interfaces [24,49].

The present study gives us an opportunity to address the impacts of these factors of the polar substrates on prenucleation in liquid light metals adjacent to the substrates. We compare the present results of the Al(l)/SiC interfaces with the interfaces of polar substrates: Mg(l)/SiC{0001} [33] and Al(l)/AlN [50] in Table 1. An idealized non-polar Al(l)/Al{111} interface [17] is included in Table 1 as a reference. All of these systems were simulated at the same temperature (T = 1000 K).

The Al(l)/Al(s) interface is idealized and non-polar [17]. It does not contain a lattice misfit, atomic roughness, or an interfacial charge transfer (a in Table 1). The prenucleation at this interface is pronounced. There are six recognizable Al layers. The in-plane coefficient of the terminating Al layer is as high as 0.50.

The AlN{0001} substrates are polarized with either an Al-(g in Table 1) or N-terminated (f in Table 1) surface [50]. The lattice misfit is large: f = −7.0%. The AIMD simulations provide strong anisotropy of the interfacial interaction and prenucleation at the interfaces. There are extra Al atoms at the terminating Al(l) layers at both Al-terminated (10%) and N-terminated (2%) interfaces, which correspond to an atomic roughness of 5.0% for the former and 1.0% for the latter (Table 1). Moreover, there are significant differences in interfacial interactions: there is a notable charge transfer from the terminating Al(l) atoms to the N in the substrate (0.52e/Al), which is opposite to the case at the Al-terminated substrate in which the terminating Al(l) atoms receive some electrons from their neighbors. The results indicate strong interfacial bonding at the Al(l)/AlN{0001}$_N$ interface and weaker bonding at the Al(l)/AlN{0001}$_{Al}$ interface. Consequently, layering at the former is strong with six recognizable layers, while it is moderate at the latter (four layers). The strong layering at the Al(l)/AlN{0001}$_N$ interface indicates a weak effect of the lattice misfit on layering, agreeing with the atomistic model [16]. The larger atomic roughness at the Al(l)/AlN{0001}$_{Al}$ interface causes it to have weaker layering. The in-plane ordering for the terminating Al layer at the Al(l)/AlN{0001}$_N$ interface is moderate (0.18) due to the large lattice misfit and atomic roughness [16]. More seriously is the in-plane-ordering at the Al(l)/AlN{0001}$_{Al}$ interface diminishing, which is caused by the combination of the large lattice misfit, atomic roughness [16,48,49], and the weak interlayer interactions [17].

Here, we compared the interfacial interactions and prenucleation of Al(l) and Mg{l} at the same SiC substrates and the Al(l)/SiC{0001} and Mg(l)/SiC{0001} [50] interfaces (Table 1). The large atomic size of Mg causes a positive lattice misfit (about 6.0%) to SiC{0001} (b and c in Table 1), whereas the lattice misfit between Al{111} and SiC{0001} is about -6.0% (d and e in Table 1). Table 1 shows that the charge transfers at the Mg(l)/SiC{0001} are notably higher than the corresponding ones at the Al(*1*)/SiC{0001} interfaces, indicating a more

ionic nature at the former interfaces. This is due to the higher electronegativity value (1.61 in Pauling scale) of Al than that of Mg (1.31). Interestingly, there are notable amounts of atomic vacancies at the terminating Mg(*l*) layers, namely 5.0% for Mg(*l*)/SiC{0001}$_C$ (b in Table 1) and 15.0% for Mg(*l*)/SiC{0001}$_{Si}$ (c in Table 1) compared with that at the Al(*l*)/SiC{0001} interfaces (d and e in Table 1). This means there are stronger effects of the atomic volume at the Mg(*l*)/SiC{0001} interfaces than at Al(*l*)/SiC{0001}. Table 1 also shows that the recognizable layers in the liquid metals at the C-terminated substrates are slightly higher than those at the Si-terminated substrates. This indicates that stronger interfacial chemical interactions enhance layering. The numbers of recognizable layers in the liquid Mg (five to six) are higher than the corresponding one in the liquid Al (three to four). This partially comes from the larger Mg interlayer space, as shown in the pronounced layering at the Mg(*l*)/Zr interfaces (seven recognizable layers) in liquid Mg [51].

Table 1. A list of the lattice misfits between the substrates and the light metals, the substrates' surface features, and prenucleation (the number of ordered layers, n_{Layers}; the in-plane-ordering of the terminating metal layers, $S_M(z)$, for the interfaces between light metals and polar substrates, Al(*l*)/SiC{0001} (this work)) (d,e), Al(*l*)/AlN{0001} reprinted from Ref. [47] (f,g), and Mg(*l*)/SiC{0001} reprinted from Ref. [33] (b,c). The related properties for the idealized L-Al/s-Al{111} interface reprinted from Ref. [17] (a) were included as a reference. * The outmost Al atoms bonded to N are classified as the terminating atoms in the AlN substrates, while they were formerly defined as the 1st Al layer in reprinted from Ref. [50].

Interface	f (%)	M Oc.(%)	R(%)	q(e/M)	n_{Layers}	$S_M(z)$	Prenucleation
a: Al(*l*)/s-Al{111} [17]	+0.0	100	0.0	0.00	6	0.50	Strong layering Strong in-plane ordering
b: Mg(*l*)/SiC{0001}$_C$ [33]	+5.9%	95	2.5	+0.50	5 to 6	0.45	Strong layering Strong in-plane ordering
c: Mg(*l*)/SiC{0001}$_{Si}$ [33]		85	7.5	+0.21	5	0.10	Strong layering Weak in-plane ordering
d: Al(*l*)/SiC{0001}$_C$ [This work]	−6.0%	100	0.0	+0.30	3 to 4	0.31	Weak layering Moderate in-plane ordering
e: Al(*l*)/SiC{0001}$_{Si}$ [This work]		103	1.5	+0.04	3	0.22	Weak layering Moderate in-plane ordering
f: Al(*l*)/AlN{0001}$_N$ [50]	−7.0%	102	1.0	+0.52	6	0.18	Strong layering Moderate in-plane ordering
g: Al(*l*)/AlN{0001}$_{Al}$ [50]		110	5.0	−0.31 *	4 *	0.02 *	Strong layering Weak in-plane ordering

Table 1 shows the relation between in-plane ordering and atomic roughness. The interfaces with smaller atomic roughness values for the C-terminated substrates have higher in-plane ordering coefficients with the Si-terminated substrates. This agrees with the previous conclusions from atomistic molecular dynamics modeling [48].

Table 1 also shows the anisotropy of chemical interactions at the interfaces between liquid metals (Mg, Al) and the polar substrates. The charge transfers from the metals to the more electronic negative atoms in the substrates (C and N) are notably larger than the values corresponding to the less electronegative atoms in the substrates (Si and Al). The obtained charge transfer between C and Al is 0.5e/Al (b), which is close to that between N and Mg at the interfaces (f). Therefore, these interactions are strong and more ionic. Meanwhile, the charge transfer from Al to C at the Al(*l*)/SiC{0001}$_C$ interface has a value of 0.3e/Al (d). This means that the bonding between Al and C at Al(*l*)/SiC{0001}$_C$ is more moderate compared with the other two, (b) and (f). The terminating Al atoms obtained 0.3e/Al on average

from the substrate Al atoms (case g in Table 1). This is caused by the strong polarity of the AlN substrate where the outmost AlN slab with Al termination donates electrons to the terminating Al atoms, which means there is strong chemical bonding between the liquid Al and the substrate in (g). The charge transfer between Mg and the Si in the substrates in (c) is still notable (0.2e/Mg). Meanwhile, the charge transfer is insignificant between the Al and Si substrates (e) in Table 1. This corresponds to the weak interaction between them from the electronic structure calculations (Figure 7). Thus, comparatively, the chemical interactions between the liquid Al and SiC substrates are moderate, indicating easier deformation and debonding between the Al matrix and the SiC substrates during machining, as shown in the literature [9–11].

Information about the chemical bonding between the light metals and the polar substrates (Table 1) is helpful to understand the wetting at the M(*l*)/solid interface. Stronger interface interactions mean smaller wetting angles. Thus, the wetting angles at the Al(*l*)/SiC interface are expected to be larger than those at the Mg(*l*)/SiC and Al(*l*)/AlN systems. However, one must also be alert that polar surfaces such as the SiC and AlN substrates are unstable at ambient conditions [13]. Such polar substrates can be stabilized by defects [52] or the absorption of small molecules [53]. This would impact wettings when added into liquid metal [54,55]. This topic deserves further investigation.

In brief, the present ab initio study revealed that the interfacial interactions at the C-terminated substrates are more significant than those at the Si-terminated substrates at the Al(*l*)/SiC{0001} interfaces. Prenucleation at the Al(*l*)/SiC{0001} interfaces is overall moderate due to the large lattice misfit and moderate interfacial interactions.

5. Conclusions

The present AIMD simulations for the interfaces between liquid Al and the polar SiC{0001} substrates provide the following results:

(i) The substrates and liquid Al at the Al(*l*)/SiC{0 0 0 1} interfaces are well separated.
(ii) The Al layers adjacent to the SiC{0001} substrates are flat with the absence of or a moderate content of atomic vacancies.
(iii) Overall prenucleation at the Al(*l*)/SiC{0001} interfaces is moderate.
(iv) There is a moderate charge transfer from the Al atoms to the outmost C (0.3e/Al), while no significant charge transfer occurs from Al to Si.
(v) The moderate interface interactions between the Al and SiC substrates indicate possible interface debonding during machining.

This study provides insights into the interfacial interactions between Al and SiC particles in and macro-mechanical performances of Al/SiC-MMCs and the role of SiC particles in the nucleation of Al metals/alloys [9,56] and other MMCs [57,58]. Furthermore, it is useful to design novel manufacturing and machining processes for nano-sized SiC-MMCs of desirable properties in practice.

Author Contributions: Conceptualization, C.F.; methodology, C.F.; software, C.F.; validation, C.F.; formal analysis, C.F.; investigation, C.F.; resources, C.F.; data curation, C.F.; writing—original draft preparation, C.F.; writing—review and editing, C.F. and Z.F.; visualization, C.F.; supervision, Z.F.; project administration, C.F.; funding acquisition, Z.F. All authors have read and agreed to the published version of the manuscript.

Funding: The financial support from EPSRC (UK) under grant number EP/V011804/1 and EP/S036296/1 is gratefully acknowledged.

Data Availability Statement: The original contributions presented in this study are included in the article. Further inquiries can be directed to the corresponding author.

Conflicts of Interest: The authors declare no conflicts of interest.

References

1. Kimoto, T.; Cooper, J.A. Chapter 2: Physical Properties of Silicon Carbides. In *Fundamentals of Silicon Carbides Technology: Growth, Characterization, Devices and Applications*; John Wiley & Sons (Pte. Ltd.): Singapore, 2014; pp. 10–37.
2. Dresch, A.B.; Venturini, J.; Arcaro, S.; Mentedo, O.P.K.; Bergmann, C.P. Ballistic ceramics and analysis of their mechanical properties for armour applications: A review. *Ceram. Intern.* **2021**, *47*, 8743–8761. [CrossRef]
3. Haynes, W.M. (Ed.) *CRC Handbook of Chemistry and Physics*, 97th ed.; CRC Press: Boca Raton, FL, USA, 2016; pp. 4–84.
4. Park, Y.-S. *SiC Materials and Devices*; Academic Press: Cambridge, MA, USA, 1988; pp. 20–60.
5. Arblaster, J.W. *Selected Values of the Crystallographic Properties of Elements*; ASM International: Materials Park, OH, USA, 2018.
6. Bekheet, N.E.; Gadelrab, R.M.; Salah, M.F.; Abd El-Azim, A.N. The effects of aging on the hardness and fatigue behavior of 2024 Al alloy/SiC composites. *Mater. Des.* **2002**, *23*, 153–159. [CrossRef]
7. Ahmed, A.; Neely, A.J.; Shankar, K.; Nolan, P.; Moricca, S.; Eddowes, T. Synthesis, tensile testing, and microstructural characterization of nanometric SiC particulate-reinforced Al 7075 matrix composites. *Metall. Mater. Trans. A* **2010**, *41*, 1582–1591. [CrossRef]
8. Atrian, A.; Majzoobi, G.H.; Enayati, M.H.; Bakhtiari, H. Mechanical and microstructural characterization of Al7075/SiC nanocomposites fabricated by dynamic compaction. *Int. J. Miner. Metall. Mater.* **2014**, *21*, 295–303. [CrossRef]
9. Wang, Y.L.; Monetta, T. Systematic study of preparation technology, microstructure characteristics and mechanical behavhors for SiC particles-reinforced metal materials composites. *J. Mater. Res. Technol.* **2023**, *25*, 7470–7497. [CrossRef]
10. Chen, Z.G.; Ding, F.; Zhang, Z.C.; Liao, Q.Y.; Qiao, Z.; Jin, Y.; Chen, M.J.; Wang, B. A review on machining SiCp/Al composite materials. *Micromachines* **2024**, *15*, 107. [CrossRef]
11. Zhao, G.L.; Mao, P.C.; Li, L.; Iqbal, A.; He, N. Micro-milling of 65 vol% SiCp/Al composites with a novel laser-assisted hybrid process. *Ceram. Intern.* **2020**, *46*, 26121–26128. [CrossRef]
12. Katkova, M.R.; Nosov, S.S.; Faddeev, M.A.; Chuprunov, E.V. On classification of silicon carbide polytypes. *Crystallogr. Rep.* **1999**, *44*, 795–798.
13. Tasker, P.W. The surface energies, surface tensions and surface structure of the alkali halide crystals. *Philos. Mag. A* **1979**, *39*, 119–136. [CrossRef]
14. Fang, C.M.; Fan, Z. Prenucleation at the liquid-Al/α-Al_2O_3 and the liquid-Al/MgO interfaces. *Comput. Mater. Sci.* **2020**, *171*, 109258. [CrossRef]
15. Fang, C.M.; Fan, Z. Atomic ordering at the interfaces between liquid Al and MgO: An ab initio molecular dynamics study. *Philos. Mag. Lett.* **2020**, *100*, 235–244. [CrossRef]
16. Men, H.; Fan, Z. Prenucleation induced by crystalline substrates. *Metall. Mater. Trans. A* **2018**, *49*, 2766–2777. [CrossRef]
17. Fang, C.M.; Men, H.; Fan, Z. Effect of substrate chemistry on prenucleation. *Metall. Mater. Trans. A* **2018**, *49*, 6231–6242. [CrossRef]
18. Fan, Z.; Gao, G.; Jiang, B.; Que, Z.P. Impeding nucleation for more significant grain refinement. *Sci. Rep.* **2020**, *10*, 9448. [CrossRef] [PubMed]
19. Zhong, Z.; Jiang, X.S.; Sun, H.L.; Wu, Z.X.; Yang, L.; Matamoros-Veloza, A. Recent research on the optimization of interfacial structure and interfacial interaction mechanisms of metal matrix composites: A review. *Adv. Eng. Mater.* **2024**, 2401392. [CrossRef]
20. Lee, J.-C.; Ahn, J.-P.; Shim, J.-H.; Shi, Z.L.; Lee, H.-I. Control of the interface in SiC/Al composites. *Scr. Mater.* **1999**, *41*, 895–900. [CrossRef]
21. Liu, P.; Wang, A.-Q.; Xie, J.-P.; Hao, S.-M. Characterization and evaluation of interface in SiCp/2024 Al composite. *Trans. Nonferrous Met. Soc. China* **2015**, *25*, 1410–1418. [CrossRef]
22. Wang, Z.; Wang, A.Q.; Han, H.H.; Xie, J.P. HRTEM study of interfacial structure in SiCp/A390 composites. *Mater. Res. Express* **2020**, *7*, 046514. [CrossRef]
23. Wang, J.S.; Horsfield, A.P.; Schwingenschlögl, U.; Lee, P.D. Heterogeneous nucleation of solid Al from the melt by TiB_2 and Al_3Ti: An ab initio molecular dynamics study. *Phys. Rev. B* **2010**, *82*, 184203. [CrossRef]
24. Fang, C.M.; Fan, Z. Ab initio molecular dynamics investigation of prenucleation at liquid- Metal/Oxide Interfaces: An overview. *Metals* **2022**, *12*, 1618. [CrossRef]
25. Liu, B.B.; Yang, J.F. Mg on adhesion of Al(111)/3C-SiC(111) interfaces from first-principles study. *J. Alloys Compd.* **2019**, *791*, 530–539. [CrossRef]
26. Xu, X.Y.; Wang, H.Y.; Zha, M.; Wang, C.; Yang, Z.Z.; Jiang, Q.C. Effects of Ti, Si, Mg and Cu additions on interfacial properties and electronic structure of Al(111)/4H-SiC(0001) interface: A first-principles study. *Appl. Surf. Sci.* **2018**, *437*, 103–109. [CrossRef]
27. Li, S.; Arsenault, R.J.; Jena, P. Quantum chemical study of adhesion at the SiC/Al interface. *J. Appl. Phys.* **1988**, *64*, 6246–6253. [CrossRef]
28. Wu, Q.J.; Xie, J.P.; Wang, A.Q.; Ma, D.Q.; Wang, C.Q. First-principles calculations on the structure of 6H-SiC/Al interface. *Mater. Res. Express* **2019**, *6*, 065015. [CrossRef]
29. Wang, C.Q.; Chen, W.G.; Xie, J.P. Calculating study on properties of Al(111)/6H-SiC(0001) interfaces. *Metals* **2020**, *10*, 1197. [CrossRef]
30. Fathalian, M.; Postek, E.; Sadowski, T. Mechanical and electronic properties of Al(111)/6H-SiC interfaces: A DFT study. *Molecules* **2023**, *28*, 4345. [CrossRef]
31. Zhang, F.; Li, Q.; Glazoff, M.V.; Ott, R.T. First-principles study of interfaces in Al/SiC metal-matrix composite system. *Comput. Mater. Sci.* **2023**, *229*, 112444. [CrossRef]

32. Wang, D.; Chen, N.X. Atomistic study of misfit dislocation in metal/SiC(111) interfaces. *J. Phys. Condens. Matter* **2010**, *22*, 135009. [CrossRef]
33. Fang, C.M.; Fan, Z. Prenucleation at L-Mg/SiC{0001} interfaces from ab initio molecular dynamics simulations. *Metall. Mater. Trans. A* **2023**, *51*, 788–797. [CrossRef]
34. Kresse, G.; Hafner, J. Ab initio molecular dynamics for liquid metals. *Phys. Rev. B* **1993**, *47*, 558–561. [CrossRef]
35. Talwar, D.N.; Sherbondy, J.C. Thermal expansion coefficient of 3C-SiC. *Appl. Phys. Lett.* **1995**, *67*, 3301–3303. [CrossRef]
36. Kresse, G.; Furthmüller, J. Efficiency of *ab-initio* total energy calculations for metals and semiconductors using a plane-wave basis set. *Comput. Mater. Sci.* **1996**, *6*, 15–50. [CrossRef]
37. Blőchl, P.E. Projector augmented-wave method. *Phys. Rev. B* **1994**, *50*, 17953–17978. [CrossRef]
38. Perdew, J.P.; Burke, K.; Ernzerhof, M. Generalized gradient approximation made simple. *Phys. Rev. Lett.* **1996**, *77*, 3865–3868. [CrossRef]
39. Monkhorst, H.J.; Pack, J.D. Special points for Brillouin-zone integrations. *Phys. Rev. B* **1976**, *13*, 5188–5192. [CrossRef]
40. Brostow, W.; Hagg Lodbland, H.E. *Materials: Introduction and Applications*; John Wiley & Sons: Hoboken, NJ, USA, 2017.
41. Hashibon, A.; Adler, J.; Finnis, M.W.; Kaplan, W.D. Atomistic study of structural correlations at a liquid-solid interface. *Comput. Mater. Sci.* **2002**, *24*, 443–452. [CrossRef]
42. Fan, Z. An epitaxial model for heterogeneous nucleation on potent substrate. *Metall. Mater. Trans. A* **2013**, *44*, 1409–1418. [CrossRef]
43. Pauling, L. The nature of the chemical bond. Application of results from the quantum mechanics and from a theory of paramagnetic susceptibility to the structure of molecules. *J. Am. Chem. Soc.* **1931**, *53*, 1367–1400. [CrossRef]
44. Bader, R.F.W.A. A quantum-theory of molecular-structure and its applications. *Chem. Rev.* **1991**, *91*, 893–928. [CrossRef]
45. Momma, K.; Izumi, F. VESTA 3 for three-dimensional visualization of Crystals, volumetric and morphology data. *J. Appl. Cryst.* **2011**, *44*, 1272–1276. [CrossRef]
46. Fan, Z. Heterogeneous Nucleation, Grain Initiation and Grain Refinement of Mg-Alloys. In Proceedings of the 11th International Conference on Magnesium Alloys and Their Applications, Sitges, Spain, 24–27 July 2018; Fan, Z., Mendis, C., Eds.; Beaumont Estate: Old Windsor, UK, 2018; p. 7.
47. Men, H.; Fang, C.M.; Fan, Z. Prenucleation at the Liquid/Substrate Interface: An Overview. *Metals* **2022**, *12*, 1704. [CrossRef]
48. Jiang, B.; Men, H.; Fan, Z. Atomic ordering in the liquid adjacent to an atomically rough solid substrate. *Comput. Mater. Sci.* **2018**, *153*, 73–81. [CrossRef]
49. Fang, C.M.; Fan, Z. Atomic ordering at the Liquid-Al/$MgAl_2O_4${111} Interfaces: Ab initio molecular dynamics simulations. *Metall. Mater. Trans. A* **2020**, *51*, 6318–6326. [CrossRef]
50. Fang, C.M.; Fan, Z. Atomic ordering at the interfaces between liquid aluminum and dipolar AlN{0001} substrates. *Metall. Mater. Trans. A* **2022**, *53*, 2040–2047. [CrossRef]
51. Fang, C.M.; Fan, Z. A Comparative Study of Prenucleation on Zr and MgO Substrates by ab initio MD simulations. In Proceedings of the 11th International Conference on Magnesium Alloys and Their Applications, Sitges, Spain, 24–27 July 2018; Fan, Z., Mendis, C., Eds.; Beaumont Estate: Old Windsor, UK, 2018; pp. 41–50.
52. Yu, L.; Zunger, A. A polarity-induced defect mechanism for conductivity and magnetism at polar-nonpolar oxide interfaces. *Nat. Commun.* **2014**, *5*, 5118. [CrossRef] [PubMed]
53. Macko, J.; Podrojková, N.; Oriňaková, R.; Oriňak, A. New insights into hydrophobicity at nanostructured surfaces: Experiments and computational models. *Nanomater. Nanotechnol.* **2022**, *12*, 18479804211062316. [CrossRef]
54. Xi, L.; Kaban, I.; Nowak, R.; Korpała, B.; Bruzda, G.; Sobczak, N.; Mattern, N.; Eckert, J. High-temperature wetting and interfacial interaction between liquid Al and TiB_2 ceramic. *J. Mater. Sci.* **2015**, *50*, 2682–2690. [CrossRef]
55. Xiao, H.Y.; Yu, Z.L.; Liang, J.C.; Ding, L.; Zhu, J.S.; Wang, Y.F.; Chen, S.G. Wetting behavior-induced interfacial transmission of energy and signal: Materials, mechanics, and applications. *Adv. Mater.* **2024**, *36*, 2407856. [CrossRef]
56. Lai, L.; Niu, B.; Bi, Y.; Li, Y.; Yang, Z. Advancements in SiC-reinforced metal matrix composites for high-performance electronic packaging: A review of thermo-mechanical properties and future trends. *Micromachines* **2023**, *14*, 1491. [CrossRef]
57. Gupta, S.; Sharma, A.K. Microstructure and Microhardness of Mg/SiC Metal Matrix Composites Developed by Microwave Sintering. *J. Inst. Eng. India Ser. C* **2022**, *103*, 63–68. [CrossRef]
58. Singh, A.; Singh, J.; Sinha, M.K. Ferrous-metal matrix composites: A review on status, scope and challenges. *Int. J. Interact. Des. Manuf.* **2023**, *17*, 2807–2829. [CrossRef]

Disclaimer/Publisher's Note: The statements, opinions and data contained in all publications are solely those of the individual author(s) and contributor(s) and not of MDPI and/or the editor(s). MDPI and/or the editor(s) disclaim responsibility for any injury to people or property resulting from any ideas, methods, instructions or products referred to in the content.